Tizian Bucher[1]
Advanced Manufacturing Laboratory,
Department of Mechanical Engineering,
Columbia University,
New York, NY 10027
e-mail: tb2430@columbia.edu

Min Zhang
Laser Processing Research Center,
School of Mechanical and Electrical Engineering,
Soochow University,
Suzhou, Jiangsu 215021, China
e-mail: mzhang@aliyun.com

Chang Jun Chen
Laser Processing Research Center,
School of Mechanical and Electrical Engineering,
Soochow University,
Suzhou, Jiangsu 215021, China
e-mail: chjchen2001@aliyun.com

Ravi Verma
Materials and Manufacturing Tech,
Boeing Research and Technology,
Berkeley, MO 63134
e-mail: ravi.verma2@boeing.com

Wayne Li
Boeing Company,
Philadelphia, PA 10027
e-mail: wayne.w.li@boeing.com

Y. Lawrence Yao
Fellow ASME
Advanced Manufacturing Laboratory,
Department of Mechanical Engineering,
Columbia University,
New York, NY 10027
e-mail: yly1@columbia.edu

Laser Forming of Metal Foam Sandwich Panels: Effect of Panel Manufacturing Method

Sandwich panels with metal foam cores have a tremendous potential in various industrial applications due to their outstanding strength-to-weight ratio, stiffness, and shock absorption capacity. A recent study paved the road toward a more economical implementation of sandwich panels, by showing that the material can be successfully bent up to large angles using laser forming. The study also developed a fundamental understanding of the underlying bending mechanisms and established accurate numerical models. In this study, these efforts were carried further, and the impact of the foam core structure, the facesheet and foam core compositions, and the adhesion method on the bending efficiency and the bending limit was investigated. These factors were studied individually and collectively by comparing two fundamentally different sandwich panel types. Thermally induced stresses at the facesheet/core interface were thoroughly considered. Numerical modeling was carried out under different levels of geometric accuracy to complement bending experiments under a wide range of process conditions. Interactions between panel properties and process conditions were demonstrated and discussed. [DOI: 10.1115/1.4043194]

Keywords: laser forming, sandwich panel, metal foam, manufacturing method, composition, numerical simulation

1 Introduction

Metal foam has long been praised for its unique properties, notably its shock and noise absorption capacity and its high strength-to-weight ratio [1]. The material can realize its fullest potential in a sandwich configuration, where the metal foam is encapsulated by sheet metal on both sides. The solid metal "facesheets" of sandwich panels not only protect the foam core from wear and tear but also create a high stiffness composite that still boasts a great shock absorption capacity while having a relatively low weight.

Many potential applications have been identified for sandwich panels with metal foam cores, ranging from parabolic mirrors in solar power plants, to rocket components and space equipment, to telescopic arms on construction equipment [2,3]. The material foremost has a great potential in the aviation industry, where it may be used for turbine casings to arrest failed turbine blades [4], for lightweight engine nacelles, or for airplane noses to absorb the shock during bird impacts [5]. In some applications, the material may even replace honeycomb structures that are widely used in airplanes nowadays, since it allows for a greater flexibility in its geometrical and structural attributes and has a uniform stiffness about all bending axes [1].

What currently hampers the implementation of sandwich panels with metal foam cores is that the material is challenging to manufacture in the shapes that are required in engineering applications. There do exist two near-net-shape methods that directly manufacture sandwich panels in nonstraight shapes. The first process is 3D printing [6], which has a limited dimensional accuracy and is only suitable for small parts with a small production volume. The second process is based on powder metallurgy. In this process, a "precursor" consisting of compacted metal and foaming agent powders is created and placed between two facesheets that are bent to the desired shape [2]. The entire assembly is placed into a mold and heated near the melting temperature of the precursor metal. The heating causes the foaming agent to release a gas that turns the precursor into a foam. Simultaneously, sintering occurs, joining the foam core to the facesheets via metallic bonds. While being convenient, this process is only suitable for relatively small parts, since it requires several molds that need to be uniformly heated. Moreover, the process is only adequate for a very large production volume, since much trial and error is required to achieve a uniform foam structure and density.

The alternative to the aforementioned processes is manufacturing the sandwich panel in a straightforward shape, such as a flat panel, and subsequently bending it to the required shape. In this fashion, panels with uniform properties can be manufactured at a lower

---

[1]Corresponding author.

cost. The challenge with this approach is that bending sandwich panels with metal foam cores is not possible with standard forming processes. Three-point bending causes many types of fractures ranging from core crushing to core failure or delamination [7]. Die stamping suffers similar defects [8], and hydroforming significantly densifies the foam core [9]. The only process that does not cause premature failures in the material is laser forming, as it is a noncontact process that induces deformation through heating and subsequent thermal expansion. The underlying bending mechanisms and numerical modeling considerations were analyzed in great detail in a previous study [10].

In Ref. [10], it was shown that laser forming can successfully bend a specific sandwich panel type, in which the facesheets and the foam core are joined directly during manufacture, discussed in detail in Sec. 2. In this study, it was investigated whether laser forming is equally capable of bending a fundamentally different sandwich panel type, in which the facesheets and the foam core are joined after having been manufactured separately. This sandwich panel type additionally has a different foam structure and facesheet type than the sandwich panel that was used in Ref. [10]. Through this analysis, it was determined whether the sandwich structure, composition, and manufacturing method have an impact on the bending mechanism, efficiency, and limit. The overarching goal of the study was to broaden the understanding of laser forming of sandwich panels with metal foam cores and to deliver the insights necessary to implement a broader variety of sandwich panels in industrial applications.

2 Background

2.1 Sandwich Panel Manufacturing Methods. In this study, two fundamentally different types of sandwich panels with metal foam cores were compared. In the first type (referred to as *Type I*, shown in Fig. 1(*a*)), the foam core and the connection between the facesheets/foam core were established in the same step. In the second type (referred to as *Type II*, shown in Fig. 1(*b*)), the foam core and facesheets were manufactured independently and joined subsequently.

Only one method may be used to manufacture sandwich panels of the first type. This method is very similar to the near-net-shape method that was mentioned in Sec. 1 [2]. A "precursor" consisting of compacted metal and foaming agent powders is placed in between solid metal facesheets and heated near the melting temperature of the precursor metal. During heating, the foaming agent releases a gas that creates bubbles, and simultaneously, the metal powders are sintered together. As the precursor expands into a foam, its lateral expansion is restricted, thereby developing a

(a)

(b)

Fig. 1 (a) Type I sandwich panel and (b) type II sandwich panel

pressure that causes the foam core to establish a metallic connection with the facesheets.

To manufacture sandwiches of the second type, many approaches may be taken to join the facesheets to the foam core. The simplest approach is to use an adhesive, which, though very affordable, is not adequate for laser forming since the adhesives cannot withstand the high temperatures that develop. The alternative is to establish metallic bonds via brazing [11] or diffusion bonding (i.e., sintering), which are generally stronger and more resistant to elevated temperatures. The latter metallic bond type was used in this study. In order to improve the bonding quality, pure aluminum powder was added between the facesheets and the foam core prior to vacuum sintering.

The advantage of type I sandwich panels is that the foam and the joints between the foam and the facesheets are created in the same step, whereas an additional joining step is required in type II sandwich panels. Also, the joint of type I sandwiches is more uniform and contains fewer defects than type II joints (as will be shown later), since the foam core does not have to be cut to the required dimensions prior to adhering it to the facesheets. At the same time, type II sandwich panels have a more uniform foam density than type I foams, whose foam density typically varies significantly. Moreover, virtually any foam geometry (open-cell, closed-cell, large/small pore) may be used in type II sandwich panels, provided that the foam composition is compatible with the facesheet and allows for diffusion bonding to occur. Type II sandwiches also do not require any molds, and the sandwich thickness can more readily be varied while still maintaining uniform foam properties.

Overall, type I sandwich panels would excel in structural applications where facesheet delamination could have catastrophic consequences. Type II sandwich panels would excel as shock absorbers where it is crucial to have consistent foam properties as well as a high flexibility in the foam geometrical attributes.

2.2 Thermally Induced Stresses at the Interface. The thermomechanical behavior of the facesheets and the foam core during laser forming is well understood. In a previous study, it was shown in great detail that the top facesheet bends via the temperature gradient mechanism (TGM) when a small laser spot size around 4 mm is used, and it bends via the buckling mechanism for large laser spot sizes around 12 mm (which turns into the upsetting mechanism (UM) in sandwich configuration). It was further shown that the metal foam bends via the modified temperature gradient mechanism (MTGM) regardless of the process condition [10]. The bottom facesheet is the only component that bends "mechanically" due to the bending moment induced by the top facesheet and the foam core. Detailed descriptions of all of the aforementioned mechanisms may be found in Ref. [12].

The behavior of the facesheet/foam core interface during laser forming, on the other hand, is comparatively poorly understood. The thermomechanical response of multilayered materials has only been studied in detail for the case where the entire composite is uniformly heated [13], which differs from the laser forming scenario where the temperature distributions are usually nonuniform. Yet, the analysis still allows for a useful comparison of the two sandwich panel types that are investigated in this study.

The stress-state at the interface can be described in terms of tractions and displacement discontinuities across the interface since both sandwich panel types have a finite yet exceedingly thin interface. Assuming that an interface of thickness η with normal and shear stiffnesses E_0, G_0 joins two layers with thicknesses s_i, thermal expansion coefficients α_i, and normal and shear stiffnesses E_0, G_0 (see Fig. 2), the normal and shear tractions t_n and t_s at the interface, respectively, become [13]

$$t_n = E_0 \frac{z_1 - z_2}{\eta} \tag{1}$$
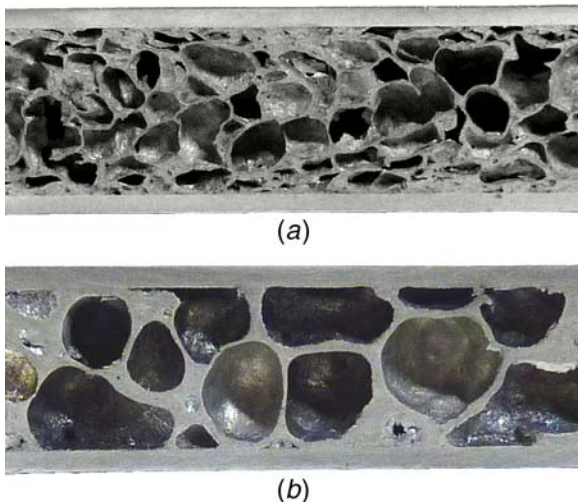
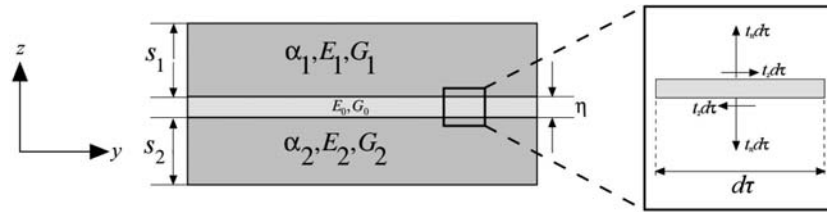$$t_s = G_0 \frac{y_1 - y_2}{\eta} \tag{2}$$

Fig. 2 Schematic of two layers of thicknesses s_1 and s_2 that are joined by an interface of thickness η, with a close-up of the traction components at the interface [13]

where y_i and z_i are the displacements of both layers in the y- and z-direction, respectively (see Fig. 2).

From Eqs. (1) and (2), it is evident that the interfacial traction magnitude increases with decreasing interface thickness η. The interface thicknesses were measured using energy dispersive X-ray spectroscopy (EDS), and it was found that the average type I interface thickness of 80 μm was smaller than the average type II interface thickness of 120 μm. An example EDS line scan of a 350 μm segment of a type I sandwich is shown in Fig. 3, where the interface can be clearly identified as the transitional zone between the low Mg-content foam core and the high Mg-content facesheet. Hence, the interfacial tractions are greater in type I sandwich panels, making them more prone to debonding. Interestingly, however, the EDS analysis also revealed that the interfacial thickness increases during laser forming. In the type I sandwich panel, for instance, the thickness increased from 80 μm to 120–130 μm after being laser formed at typical process conditions. Therefore, laser forming seems to alleviate the stress concentration at the interface by promoting more intermetallic diffusion.

The displacement discontinuities in Eqs. (1) and (2) can be determined from the following equations, assuming that the displacements are infinitesimally small and only arise due to uniform heating of the facesheet and the foam core

$$\frac{dy_i}{d\tau} = \alpha_i \Delta T + \frac{P_i}{ws_i E_i} + \frac{s_i}{2R} \tag{3}$$

$$\frac{d^2 z_i}{d\tau_i^2} = -\frac{12(1 - v_i^2)M_i}{E_i s_i^3} \tag{4}$$

where $d\tau$ is the width of the section over which the force analysis is performed (see Fig. 2) and v_i is Poisson's ratio. The first term

in Eq. (3) represents the thermal expansion in the y-direction of each layer due to the heating by ΔT. The second term in Eq. (3) is due to the load P_i that arises in both layers (compressive in one and tensile in the other) because the layers are unable to slide past each other. w refers to the specimen width. The third term in Eq. (3) is due to the moments M_i that the layers exert onto each other since the radius of curvature R at the interface differs from the radii that the two layers strive to follow. These moments M_i also cause a displacement discontinuity in the z-direction, shown in Eq. (4), since they would cause each layer to bend by a different amount if the layers were separated [13].

From Eqs. (1)–(4), it can be seen that substantial displacement discontinuities arise due to the different thicknesses of the foam core (8 mm) and the facesheets (1 mm). The equations further show that the displacement discontinuities, and hence the interfacial stresses, increase the more, the material properties of the foam core and the facesheets differ. Based on this, the interfacial stresses are again predicted to be higher in the type I sandwich panel, where the AlSi10 foam core properties substantially differ from the AW 5005 facesheet properties, than in the type II sandwich panel where both the foam core and the facesheets consist mostly of aluminum ($\geq$99.6 wt %).

Based on this theoretical analysis, the type I sandwich panel is more susceptible to develop high interfacial stresses that could lead to delamination. In reality, however, no delamination occurred during laser forming in either sandwich type as will be shown later. Therefore, the diffusion-based metallic bonds of the sandwich panels are strong enough to withstand the stresses caused by laser heating. This might in part be due to the ongoing intermetallic diffusion that occurs during laser forming.

2.3 Numerical Simulation. Three types of numerical models were used in this study, which may be grouped into the categories of *equivalent sandwich models* and *explicit sandwich models*. Equivalent sandwich models (Fig. 4(a)) approximate the foam geometry as a rectangular box and use metal foam material properties. Since metal foam is able to yield both due to shear stresses (Von Mises equivalent stress σ_e) as well as due to hydrostatic stresses σ_m, the yield criterion becomes [14]

$$F = \left[\frac{1}{1 + (\beta/3)^2} (\sigma_e^2 + \beta^2 \sigma_m^2) \right]^{1/2} - Y \leq 0 \tag{5}$$

where Y is the yield strength and β is the aspect ratio of the yield surface. When $F < 0$, elastic deformation occurs, while $F = 0$ initiates plastic deformation following the flow rule

$$\dot{\varepsilon}_{ij}^p = \frac{\dot{Y}}{H} \frac{\partial F}{\partial \sigma_{ij}} \tag{6}$$

where $\dot{\varepsilon}_{ij}^p$ is the plastic strain rate and H is the hardening modulus defined as

$$H = \frac{\sigma_e}{\hat{\sigma}} h_\sigma + \left(1 - \frac{\sigma_e}{\hat{\sigma}} \right) h_p \tag{7}$$

where h_σ and h_p are the tangent moduli in uniaxial and hydrostatic compression, respectively, and $\hat{\sigma}$ is equal to the first term in Eq. (5).
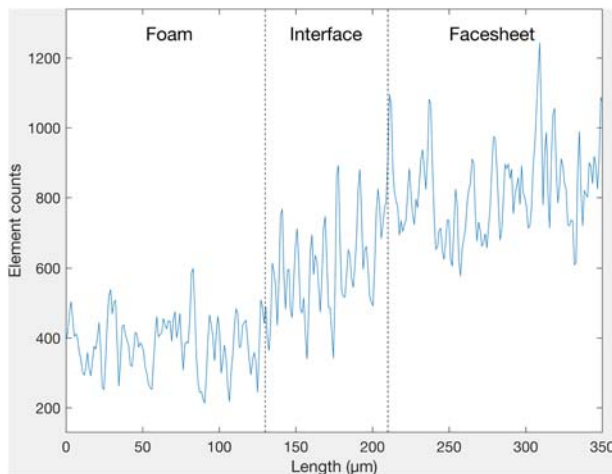

Fig. 3 Typical EDS line scan of a type I sandwich panel specimen, showing the magnesium content. The scan was performed across the interface between the facesheet and the foam core. The interface is the intermediary region between the high Mg-content facesheet and the low Mg-content foam.
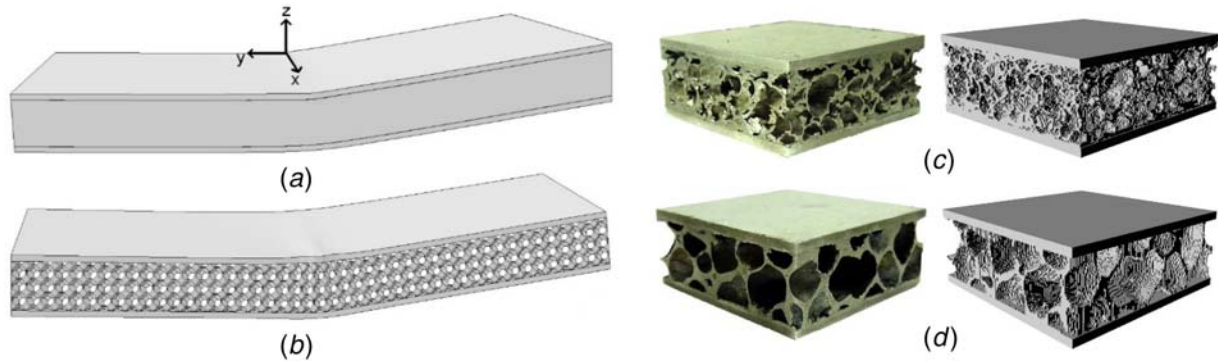
Fig. 4 (*a*) Equivalent sandwich model, (*b*) Kelvin-cell sandwich model, (*c*) type I sandwich panel specimen (left) and corresponding voxel model (right), and (*d*) type II sandwich panel specimen (left) and corresponding voxel model (right)

The assumptions of the model were discussed in detail in a previous study [15]. In the finite element code ABAQUS that was used in this study, this constitutive model is incorporated as *foam crushable model*. The mesh that was used for the foam model is shown in Fig. 8 and discussed in detail in Refs. [15,16].

Explicit models, in contrast, directly model the foam structure and use the bulk properties of the metal that comprises the foam (AlSi10 for type I and Al 99.7 for type II). Hence, they are governed by a constitutive model that describes the behavior of bulk metals. Similar to many previous laser forming studies [17], the deformation is assumed to be incompressible, and Von Mises' yield criterion, the Von Mises flow rule, as well as strain hardening are assumed to hold. Two types of explicit models were used in this study, which are discussed in detail in Refs. [15,16]. The first model, called *Kelvin cell sandwich model* (Fig. 4(*b*)), approximates the shape of a single cavity by a Kelvin cell geometry and assumes the wall thickness to be constant throughout. The model was obtained by cutting arrays of Kelvin cells out of a solid block. The second explicit model that was used is a *voxel sandwich model*. It was obtained by performing a micro-computed tomography (CT) scan of 25 mm by 25 mm sandwich panel specimens at a resolution of 30 μm and by converting high absorption points of the data cloud to cubical volumes that are called *voxels*. The resolution was then manually reduced to 150 μm in order to reduce the number of elements to around 400,000. Figure 4(*c*) shows a voxel model of the type I sandwich panel, next to the original, and Fig. 4(*d*) shows a voxel model of the type II sandwich panel. Due to their reduced size, the voxel models were only used for a qualitative analysis in this study.

In all three models, the facesheets were modeled as incompressible solids that follow Von Mises' yield criterion. In the equivalent and Kelvin sandwich models, 3 and 2 elements were used through the thickness of the top and bottom facesheets, respectively. In the voxel models, 4 and 3 elements were used, respectively, due to the finer mesh of the foam.

The interface between the facesheets and the foam was modeled using cohesive elements. The stress-state was described in terms of tractions and displacement discontinuities that were linearly related via the stiffness matrix K

$$\begin{bmatrix} t_n \\ t_s \\ t_t \end{bmatrix} = \begin{bmatrix} K_{nn} & 0 & 0 \\ 0 & K_{ss} & 0 \\ 0 & 0 & K_{tt} \end{bmatrix} \begin{bmatrix} u_n \\ u_s \\ u_t \end{bmatrix} \quad (8)$$

where the subscripts n, s, and t refer to the normal, first, and second shear directions, respectively. All stiffness components of the cohesive elements were set to a very large value (80 GPa) to ensure that the overall sandwich stiffness is unaffected by the presence of the interface [18].

All the simulations were performed in an uncoupled manner, using the results of the heat transfer analysis as input to the mechanical analysis. For the heat transfer analysis, DC3D20, DC3D10, DC3D8 elements were used for the equivalent, Kelvin, and voxel foams, respectively, and C3D20R, C3D10, and C3D8R elements were used for the mechanical analysis. For the facesheet, DC3D20 and C3D20R elements were used for the heat transfer and mechanical analysis, respectively. DC3D8 and COH3D8 elements were used for the cohesive elements during the thermal and mechanical analyses, respectively.

The material properties for the type I foam (AlSi10) were extracted from Ref. [19], and the properties for the AW 5005 facesheet (AlMg1) were extracted from Ref. [20]. For the type II sandwich, Al 99.7 properties from Ref. [21] were used both for the facesheet and the foam core. An absorption coefficient of 0.6 was used. The laser source was modeled with the user subroutine *dflux*.

3 Experimental Methods

Two sandwich panel types were used in this study, whose manufacturing methods were explained in detail in Sec. 2.1. The type I sandwich panel was manufactured by Havel Metal Foam GmbH, and the type II sandwich panel was manufactured at the Northeastern University in China. To maximize the scope of this study, the type I and type II sandwich panels additionally consisted of different facesheet types and foam structures. In the type I sandwich panel, the facesheets were made of AW 5005, containing Magnesium as a major alloy element. The foam core was made of AlSi10 and had an average cavity size of roughly 2 mm. In the type II sandwich panel, both the facesheet and the foam had a high aluminum content ($\geq$99.6 wt %), with the facesheet being made of Al 1060. In both sandwich panel types, the facesheet thickness was 1 mm. The foam core was manufactured using the melt foaming method [22], using TiH_2 as the foaming agent and having an average cavity size of roughly 4 mm. The foam cores of both sandwiches had an average density around 700 kg/m^3 (74% porosity) and a thickness of 8 mm.

Laser forming experiments were performed using a CO_2 laser with a wavelength of 10.6 μm. The specimen surfaces were coated with black graphite paint to maximize the laser absorption. Between successive laser scans, the specimens were allowed to cool back to room temperature. The specimens were scanned in the x-direction shown in Fig. 4(*a*), and the deflection was measured using a dial indicator.

Two process conditions, which were also used in a previous study [10], were investigated. In the first process condition, a large spot size of 12 mm was used with a slow scan speed of 10 mm/s. In the second process condition, a small spot size of 4 mm was used with a fast scan speed of 30 mm/s. The power was set to 800 W for both conditions to maintain a constant area energy.

An infrared camera was used to measure the bottom surface temperature of the sandwich panels during laser forming. The frame rate of the camera was 120 Hz (8 ms per frame), and the spatial

resolution was roughly 0.1 mm. The specimens were placed above an aluminum shield to prevent the laser irradiation from damaging the IR camera. The measured surfaces were coated with highly emissive black graphite paint ($e = 0.92$) to maximize the measurement accuracy, and the results were averaged over a diameter of 1 mm.

4 Results and Discussion

4.1 Bending Efficiency and Limit. This study was initiated by investigating the impact of the sandwich composition and manufacturing process on the bending behavior, specifically the bending efficiency and the maximum achievable bending angle. Both sandwich panel types were laser formed at a small laser spot size ($D = 4$ mm, $v = 30$ mm/s) and a large laser spot size ($D = 12$ mm, $v = 10$ mm/s), and the bending angles were recorded over 8 scans (Fig. 5). At $D = 4$ mm, the two sandwich panel types bent by about the same amount over 8 laser scans. Also, the maximum achievable bending angle was similar, being ∼15 deg for the type I panel and ∼12 deg for the type II panel. At $D = 12$ mm, on the other hand, the type I panel bent at a much higher rate than the type II panel. Moreover, the maximum achievable angle was around 65 deg (Fig. 6(a)), while the maximum angle was ∼45 deg for the type II panel (Fig. 6(b)).
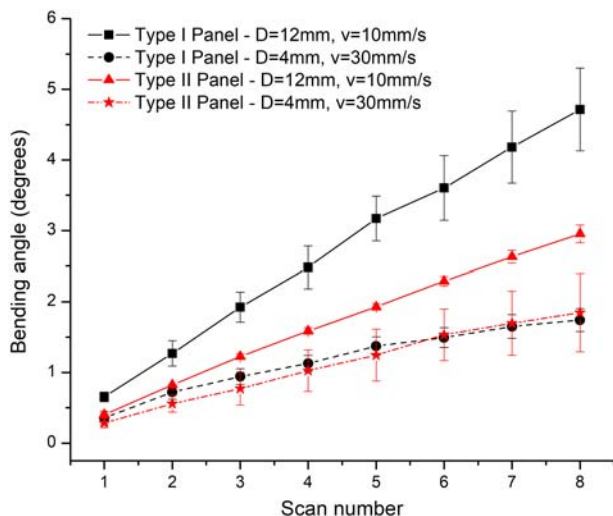

Fig. 5 Bending angles of both sandwich panel types over 8 laser scans at a large spot size ($D = 12$ mm, $v = 10$ mm/s) and a small spot size ($D = 4$ mm, $v = 30$ mm/s), the power was constant at $P = 800$ W. The results were averaged over three specimens; standard errors are shown.
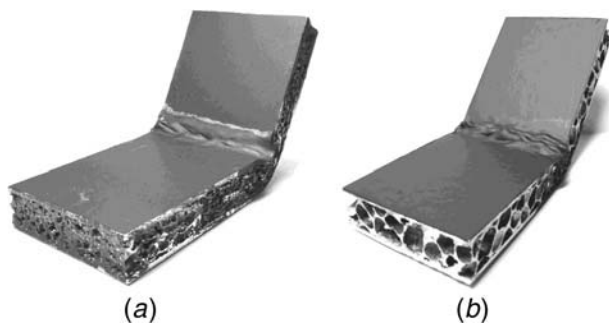

Fig. 6 The bending limit of the (a) type I and (b) type II sandwich panel at a large spot size ($D = 12$ mm, $v = 10$ mm/s) were around 65 deg and around 45 deg, respectively. In the type I sandwich panel, the top facesheet mostly deformed inwards, whereas it mostly deformed outwards in the type II sandwich panel.

Hence, some attribute(s) of the sandwich panels caused a significant deviation in the efficiency and bending limit at a large spot size. Due to the numerous differences between the sandwich panel types, a series of experiments and numerical studies were performed to identify the cause(s) of the aforementioned deviations.

4.2 Effect of Facesheet. The impact of the facesheet composition was investigated first. The type I (AW 5005) and type II (Al 1060) facesheets hardly differ in their thermal properties, but they have two notable differences in their mechanical properties. First, the yield strength of the type I facesheet is almost twice the yield strength of the type II facesheet. Second, the type II facesheet undergoes substantially more softening than the type I facesheet at elevated temperatures. Intuitively, one would expect the type II sandwich to bend more, due to its softness. Laser forming experiments of "isolated" facesheets (facesheets that were cut from the sandwich panel) showed the opposite (Fig. 7), however, an unintuitive result that is characteristic to laser forming. The TGM that is induced at this process condition ($D = 4$ mm, $v = 30$ mm/s) relies on the fact that the thermal expansion of the heated material is restricted by the "cold" surrounding material, a condition that is better satisfied by a stiff material such as AW 5005, and less so by a material that undergoes substantial thermal softening such as Al 1060.

The same explanation applies when the entire sandwich panel is bent at a large spot size of $D = 12$ mm: the facesheet deformation via the UM is more efficient if the thermal expansion of the heated material is restricted by the "cold" surrounding material, which is again better satisfied by the type I facesheet. Numerical simulations confirmed this by showing that the plastic compressive strain in the y-direction is much greater for the type I facesheet (Fig. 8(a)) than in the type II facesheet (Fig. 8(b)). The simulations also showed that the sandwich panel with type I facesheet properties bent by 0.68 deg, when compared with the sandwich panel with type II facesheet properties that only bent by 0.56 deg (leaving all remaining properties the same).

Overall, the facesheet comparison showed that the type I facesheet bends at a higher rate than the type II facesheet, which is partially responsible for the difference in the bending efficiency in Fig. 5. However, the difference between the deformation behavior of the facesheets is relatively small and does not fully explain why the two sandwich panel types responded vastly different at $D = 12$ mm in Fig. 5. Therefore, there are other factors that more significantly influenced the bending efficiency.
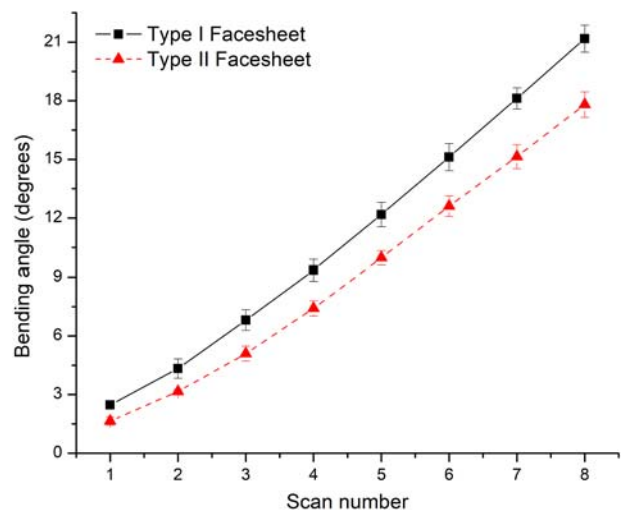

Fig. 7 Bending angles of the "isolated" facesheets (not attached to foam core) at a small spot size ($D = 4$ mm, $v = 30$ mm/s). The type I facesheet, made of AW 5005, bent more efficiently than the type II facesheet, which was made of Al 1060.
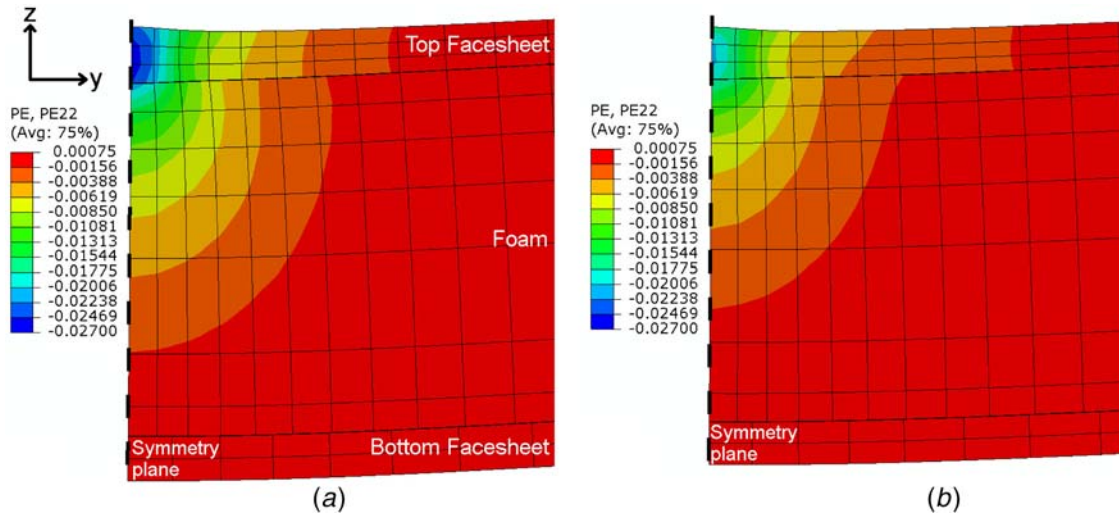
Fig. 8 Plastic strain distribution in the y-direction after a laser scan at (D = 12 mm, v = 10 mm/s). AW 5005 facesheet properties were used in (a), and Al 1060 facesheet properties were used in (b). The remaining geometrical and material properties were identical. The deformation was scaled by a factor of 10 for viewing clarity. Only half of the model is shown due to symmetry.

4.3 Effect of Foam Core. The next component that was analyzed was the foam core. From a thermal standpoint, the two foams behave very similarly, as can be seen from their thermal response in Fig. 9. The results were obtained by machining two cylindrical foam pucks with a diameter of 25 mm and a thickness of 6 mm for both foam types. All the tested pucks had a similar density and surface area, and they were tested in both directions (four tests per foam type). The pucks were placed between mirror-polished aluminum disks with a thickness of 1 mm (see diagram in Fig. 9). The assembly was clamped in a holder, a laser source with a diameter of $D = 12$ mm was applied to the top surface, and the temperature history was recorded on the bottom surface using an IR camera. The exposed surfaces of the aluminum disks were spray-painted with black graphite paint to increase the laser absorption (top) and to ensure a high emissivity (bottom). The results in Fig. 9 show that the heat diffusion is very similar
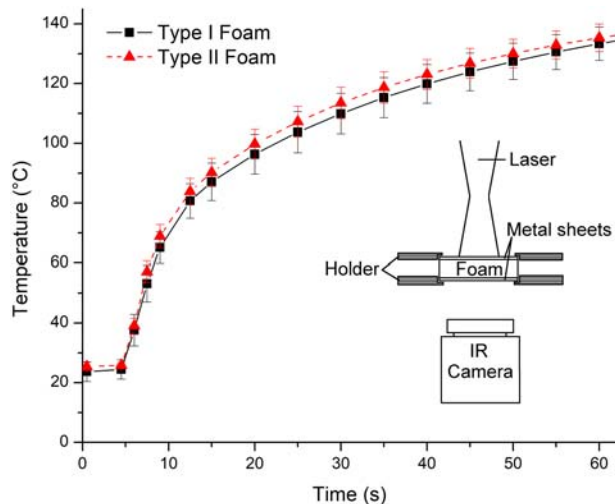
through both foam types, despite the fact that their structures are fundamentally different.

From a mechanical standpoint, the two foam types do not differ significantly either. The type I foam consists of an AlSi10 alloy and has a higher strength than the high aluminum-content type II foam ($\geq$99.6 wt %). Hence, the type I foam is expected to bend more efficiently during laser forming. This effect is canceled out by the fact that the moment of area of the type I foam is on average 18% higher than the moment of area of the type II foam (Fig. 10), making it more resistant to bending deformation. The moment of area was calculated for each pixel of a particular micro-CT slice using the following relation:

$$I = \int_{-s/2}^{s/2} z^2 y(z)dz \qquad (9)$$

where s is the sheet thickness. The individual moments were then summed up using the parallel axis theorem. The moment of area was calculated about a horizontal axis at the center of specimens (not shown in Fig. 10).

Based on all the above results, both the thermal and mechanical responses of the type I and II foams are very similar. Therefore, the foam core behavior cannot possibly be the reason for the different bending efficiencies and bending limits observed in Figs. 5 and 6.

4.4 Thermal Response of Sandwich Panel. Neither the facesheets nor the foam cores are the major cause of the different behavior of the type I and II sandwich panels. Hence, the two sandwich panel types must differ in the way that their facesheets and foam cores interact. This interaction occurs on a thermal as well as a mechanical basis. The thermal interaction was investigated first by scanning both sandwich panel types at a small spot size ($D = 4$ mm, $v = 30$ mm/s) as well a large spot size ($D = 12$ mm, $v = 10$ mm/s) and by recording temperature on the bottom sandwich surface using an IR camera, shown in Fig. 11. For both sandwich types, the bottom surface reached higher temperature values at a larger spot size and a slower scan speed. This finding is consistent with previously reported results and relates to the fact that more heat diffusion can occur at slow scan speeds [16,23]. Figure 11 also shows that the type I sandwich panel reached slightly higher temperature magnitudes than the type II sandwich panel, which can be attributed to two causes. First, the facesheet adhesion quality is superior in type I sandwich panels, as will be shown later. Second, the type I foam

Fig. 9 Foam pucks were sandwiched between two solid aluminum disks. A laser with spot size D = 12 mm was applied to the top surface of the assembly and the temperature was measured underneath. The measured heat diffusion through the type I and type II foams was very similar. The results were averaged over two specimens that were tested from both directions, standard deviations are shown.

	Cross-section	Moment of area
Type I Foam		1.18
Type II Foam		1

Fig. 10 The moment of area of the type I foam is on average 18% greater than the moment of area of the type II foam, making it stiffer to bending deformation
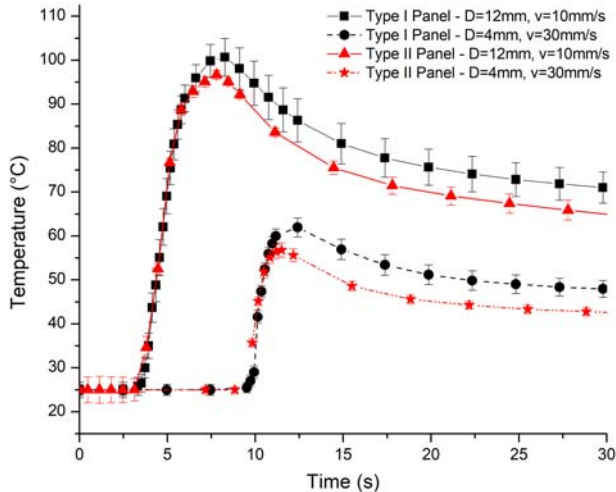

Fig. 11 Temperature history on the bottom surface of the sandwich panels during laser scans at a large spot size ($D = 12$ mm, $v = 10$ mm/s) and a small spot size ($D = 4$ mm, $v = 30$ mm/s). Four specimens were tested for each sandwich panel type, standard deviations are shown.

is denser near the facesheets, allowing for an increased heat transfer between the top facesheet and the foam compared with the type II sandwich panel. Overall, the temperature difference between the two sandwich types was rather insignificant; however, considering that their top surfaces were heated up to 600 °C.

Numerical simulations confirmed that the thermal response of both sandwich panel types is similar. Figures 12(a) and 12(b) show the temperature distributions in the type I and type II sandwich

panels during a laser scan at $D = 12$ mm and $v = 10$ mm/s performed using voxel models. The same temperature-dependent gap conductance relationship was used at the interface for both panels, discussed in detail in Ref. [10]. As was mentioned previously, heat can flow rather continuously from the top facesheet to the foam core in the type I sandwich panel (Fig. 12(a)) due to the small cavity size and the high foam density near the facesheets, whereas its flow is restricted to the sparsely spaced cell walls in the type II sandwich panel (Fig. 12(b)). As a consequence, the top facesheet heated up slightly more in the type II sandwich panel. Nevertheless, the thermal behavior of the two sandwich panel types was similar and must not have been the cause for the different bending efficiencies and bending limits.

4.5 Mechanical Response of Sandwich Panel. Having ruled out the differences in the facesheets, the foam core as well as the thermal interaction between the facesheets and foam core as major causes of the discrepancies in Figs. 5 and 6, the mechanical interaction of the facesheets and foam core is the last possible option. Results confirmed that the foam core structure is the key factor deciding how the facesheets and the foam core interact, thereby defining the bending behavior of the entire sandwich. While the type I foam core consists of many thin cell walls that can readily crush when subjected to compressive stresses, the type II foam core consists of fewer thick cell walls that only bend when subjected to very high compressive stresses. One consequence of this is that the deformation via the MTGM is less efficient in the type II foam. The second and more important consequence is that the top facesheet starts behaving differently during laser forming.

In the type I sandwich panel, the top facesheet can readily penetrate into the foam core, both at small spot sizes (Fig. 13(a)) and large spot sizes (Fig. 13(c)), due to the high crushability of the
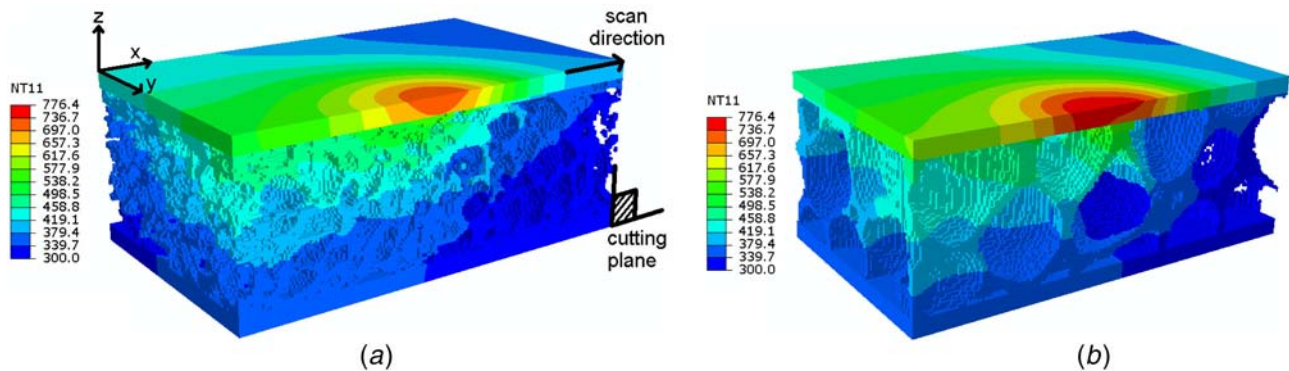

Fig. 12 Temperature distribution in voxel models of (a) type I sandwich panels and (b) type II sandwich panels, during a scan at a large spot size ($D = 12$ mm, $v = 10$ mm/s). The laser was scanned in the x-direction. The models were sliced along the laser scan line for viewing clarity.
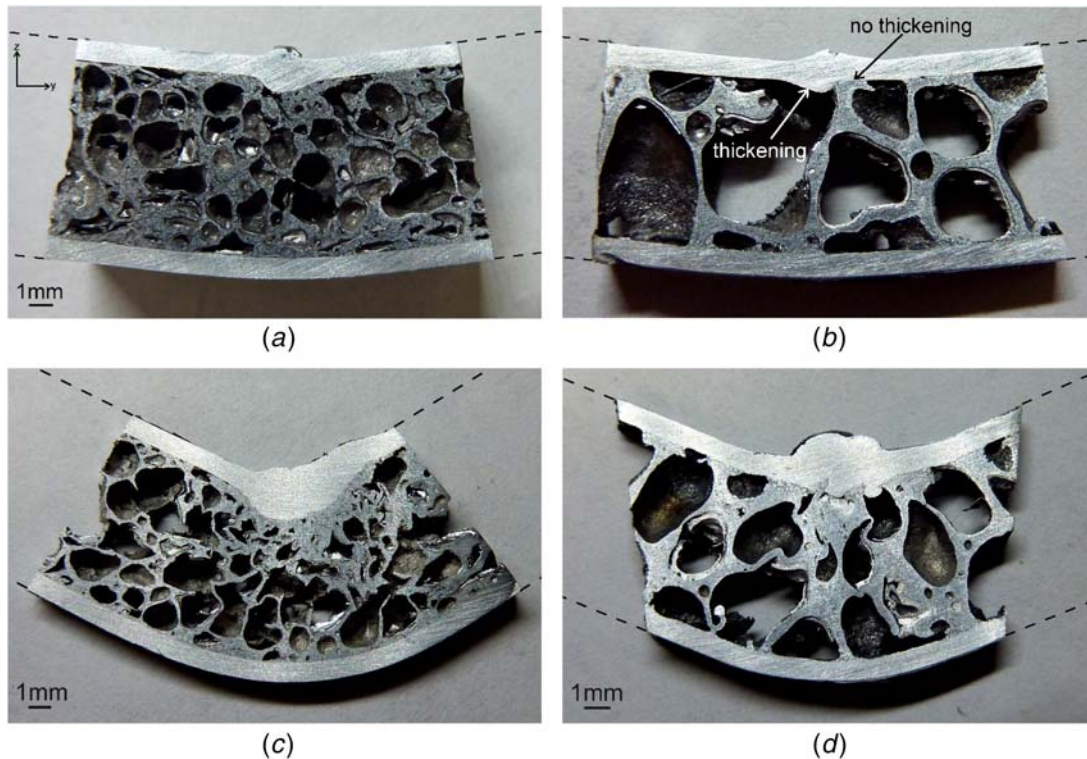
Fig. 13 Cross sections of type I and type II sandwich panels that were bent to the bending limit. The laser was scanned into the page. At a small spot size ($D = 4$ mm, $v = 30$ mm/s), (a) the bending limit of the type I sandwich panel is around 15 deg and (b) for the type II sandwich panel it is around 12 deg (b). At a large spot size ($D = 12$ mm, $v = 10$ mm/s), the limit is (c) around 65 deg for the type I sandwich panel, and (d) around 45 deg for the type II sandwich panel.

foam core. In the type II sandwich, on the other hand, the top facesheet can penetrate into the foam core if a cavity is underneath, but not if a cell wall is underneath. Figure. 13(b) highlights this point, showing an example where the deformation at the scan line (in the center) is strictly divided between a left segment where the facesheet was able to thicken downward (in negative z-direction) due to a cavity and a right segment where no downward thickening occurred due to the presence of a cell wall.

This facesheet thickening behavior has a relatively minor impact on the bending efficiency and maximum bending angle at a small spot size of $D = 4$ mm, because the facesheet deformation via the TGM is relatively localized. At large spot sizes of $D = 12$ mm, however, the facesheet deformation is more widespread due to the UM, and the behavior of the top facesheet becomes more important. Unlike in the type I sandwich panel (Fig. 13(c)), where the top facesheet could significantly penetrate into the foam core, the top facesheet could hardly penetrate into the foam core in the type II sandwich panel (Fig. 13(d)). Instead, most of the facesheet deformation occurred in an outward direction (positive z-direction). As a consequence, the overall thickness of the type II sandwich panel increased tremendously, rendering the sandwich stiffer and limiting the maximum achievable bending angle. The type I sandwich panel (Fig. 13(c)), in contrast, maintained almost the same thickness, allowing deformation up to larger bending angles.

Numerical simulations with voxel models qualitatively illustrate this point. Figures 14(a) and 14(b) show the plastic compressive strains in the y-direction in a type II sandwich panel after a single laser scan at $D = 12$ mm, $v = 10$ mm/s, and $P = 800$ W. Case (a) represents a scenario where a cavity is situated underneath the facesheet (by the scan line) and is contrasted with case (b), where a cell wall is located underneath the facesheet. In (a), the facesheet is able to thicken in downward direction, and high plastic strain magnitudes are reached due to the efficient action of the UM. In (b), the facesheet can only thicken in the upward direction, the

UM becomes less efficient, and lower plastic strain magnitudes are reached.

This effect can also be quantified using a Kelvin-cell model. In Fig. 15(a), the Kelvin-cell foam core was aligned such that most of the space underneath the top facesheet was occupied by cavities (representing case (a) from above). In Fig. 15(b), the Kelvin-cell foam core was aligned such that cell walls were located directly underneath the top facesheet (representing case (b) from above). All other parameters and geometrical properties were identical. The first scenario yielded a bending angle of 0.81 deg at the same condition as in Fig. 14, and the second scenario yielded a bending angle of only 0.73 deg. The simulation further yielded the same facesheet thickening behavior and plastic compressive strain distributions as the voxel models in Fig. 14.

Overall, the previously shown results demonstrate that the foam structure of the type II restricts the downward expansion of the top facesheet. As a result, the top facesheet thickens mostly in an upward direction and bends less efficiently. This result is amplified at large laser spot sizes where the deformation region is large. Moreover, the maximum achievable bending angle is reduced, because the upward facesheet thickening increases the overall sandwich panel thickness and renders the sandwich more resistant to bending deformation.

4.6 Importance of Facesheet Adhesion Quality. In Sec. 4.5, it was shown that the foam core structure has a significant impact on the maximum achievable bending angle. The interface adhesion quality has an even greater impact on the bending limit. If the facesheets are completely bonded to the foam core via metallic diffusion bonds, large bending angles of 65 deg (type I sandwich panel) and 45 deg (type II sandwich panel) can be achieved, since laser forming does not cause any delamination. This fact can readily be accepted, looking at Fig. 13, where the adhesion between the
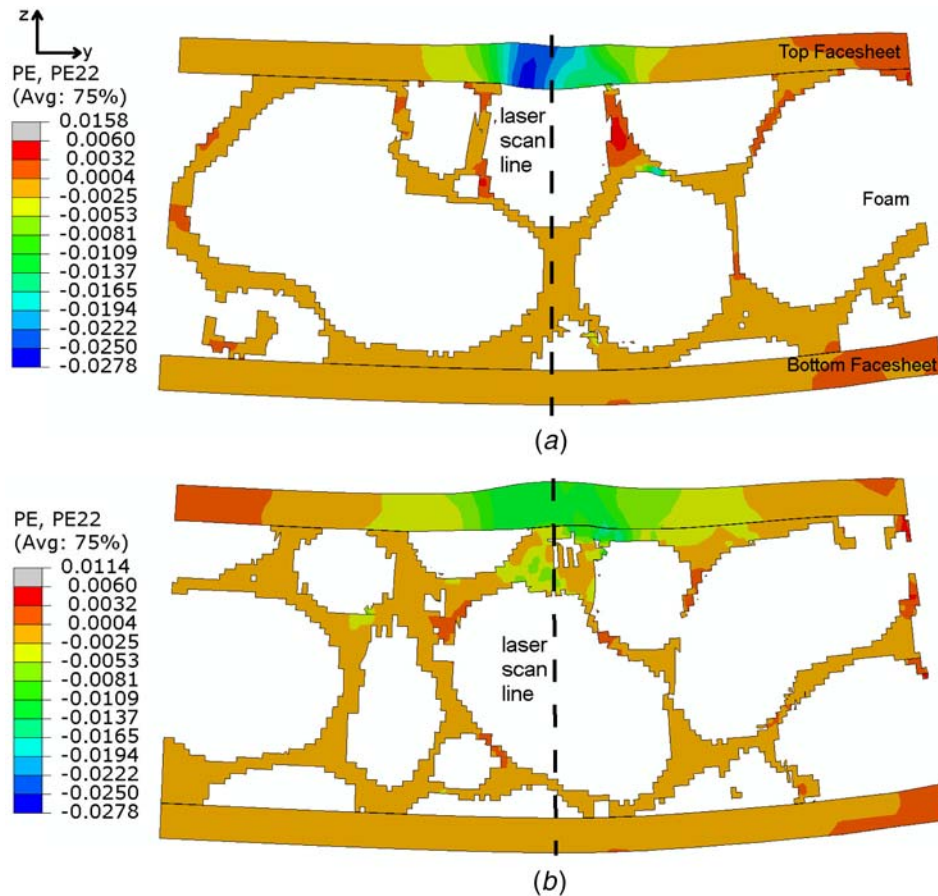
Fig. 14 Plastic strain distributions in the *y*-direction in a type II sandwich panel after a laser scan at a large spot size (*D* = 12 mm, *v* = 10 mm/s), shown using a voxel model. The deformation was scaled by a factor of 10 for viewing clarity. The laser was scanned into the page, and the laser center was on the dashed line.
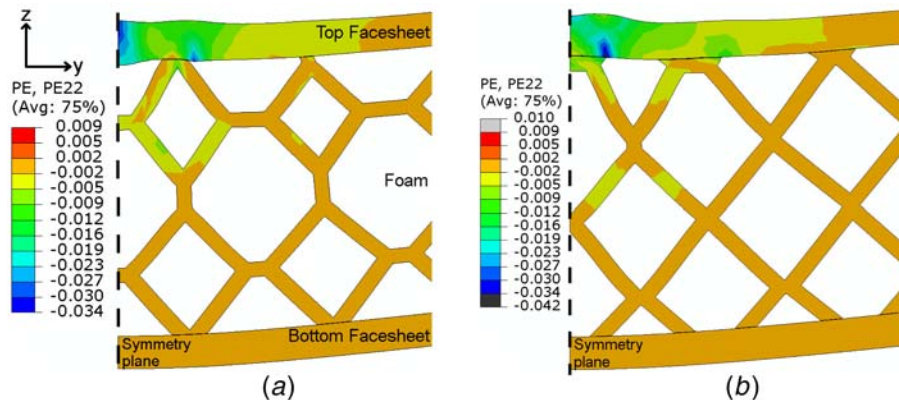

Fig. 15 Plastic strain distributions in the *y*-direction in a Kelvin-cell sandwich model after a laser scan at a large spot size (*D* = 12 mm, *v* = 10 mm/s). Only half of the model is shown due to symmetry. In (*a*), the foam core was constructed such that cavities are underneath the top facesheet at the symmetry plane, whereas in (*b*), mostly cell walls are underneath the top facesheet. The remaining properties of both models are identical. The deformation was scaled by a factor of 10 for viewing clarity.

facesheets and the foam core remained perfectly intact despite all the contortions of the top facesheet.

If, on the other hand, the facesheet adhesion is poor and there are regions of detachment after manufacture, the maximum achievable bending angle plummets. Pre-existing detachment has not been observed in the type I sandwich panel, as the adhesion quality is generally high due to the diffusion bonds being created during the formation of the foam core. In the type II sandwich panel, however, regions of pre-existing detachment do occur, as shown in Fig. 16(*a*). The reason why the type II sandwich is more prone to having pre-existing detachment is that the foam core and the interfacial adhesion are created in separate steps. During cutting
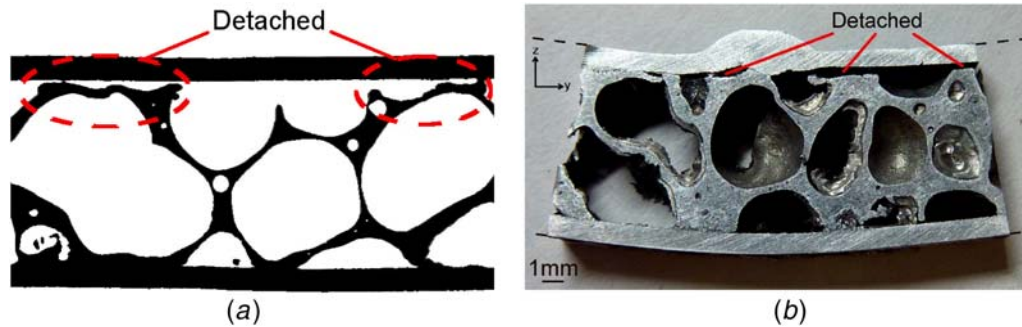
Fig. 16 (a) A cross section of the type II sandwich panel obtained using a micro-CT scan shows that there are regions of detachment between the facesheet and the foam core. This detachment is detrimental to laser forming since the maximum achievable bending angle drops from 45 deg to around 15 deg at a large spot size ($D = 12$ mm, $v = 10$ mm/s), shown in (b).

and handling the foam core might get locally damaged, so that it no longer is in contact with the facesheets during sintering. Gaps between the facesheets and the foam core may also occur if the pressure during the sintering step is not applied uniformly.

Given a situation with pre-existing detachment, the bending limit dropped from 45 deg (Fig. 13(d)) to merely 15 deg (Fig. 16(b)). Several factors are responsible for this significant drop in the bending limit. First, pre-existing detachment decreases the heat transfer from the top facesheet to the rest of the sandwich, reducing the temperature gradient in the foam core as well as its contribution to bending via the MTGM. Second, the bottom facesheet heats up less and undergoes less heat-induced softening. Finally, the top facesheet is completely unable to penetrate into the foam core. It was mentioned previously that the top facesheet penetrates less into the foam core in the type II sandwich panel than in the type I sandwich panel, but it still penetrates to some extent as can be seen in Fig. 13(d). In the detached case, however, the facesheet entirely thickens away from the foam core (positive z-direction), increasing the sandwich panel thickness and rendering it more resistant to bending deformation.

Numerical simulations again support the aforementioned arguments. Using an equivalent model, a case with perfect adhesion (Fig. 17(a)) was contrasted with a case where the top facesheet was detached from the foam core over half the beam spot size of $D = 12$ mm (Fig. 17(b)). In the detached case, the top facesheet underwent more heating and thus developed greater plastic compressive strains in the y-direction. At the same time, the plastic

compressive strain distribution in the foam core was reduced near the laser scan line, indicating less efficient bending via the MTGM [15]. The simulations also confirmed that the top facesheet only thickened in an upward direction (positive z-direction) in the detached case, whereas it thickened in both directions in the intact case.

5 Conclusions

This study comparatively studied the behavior of two types of sandwich panels with metal foam cores during laser forming. They differed in the facesheet type, foam core structure, and composition, as well as the adhesion method. It was shown that the two sandwich panel types have a similar bending efficiency and bending limit when formed at small laser spot sizes ($D = 4$ mm). At large laser spot sizes ($D = 12$ mm), it was shown that type I sandwich panels bend at a much higher rate and achieve a higher bending angle.

Two major causes were identified for this discrepancy. First, it was shown that the type I facesheet bends at a higher rate, owing to its increased strength and stiffness. Second, it was demonstrated that the foam core structure determines how the top facesheet thickens during laser forming. In the type I sandwich panel, the top facesheet can penetrate into the foam core, allowing for a more efficient deformation via the upsetting mechanism. In the type II sandwich panel, on the other hand, the top facesheet mostly thickens away from the foam core, increasing the overall
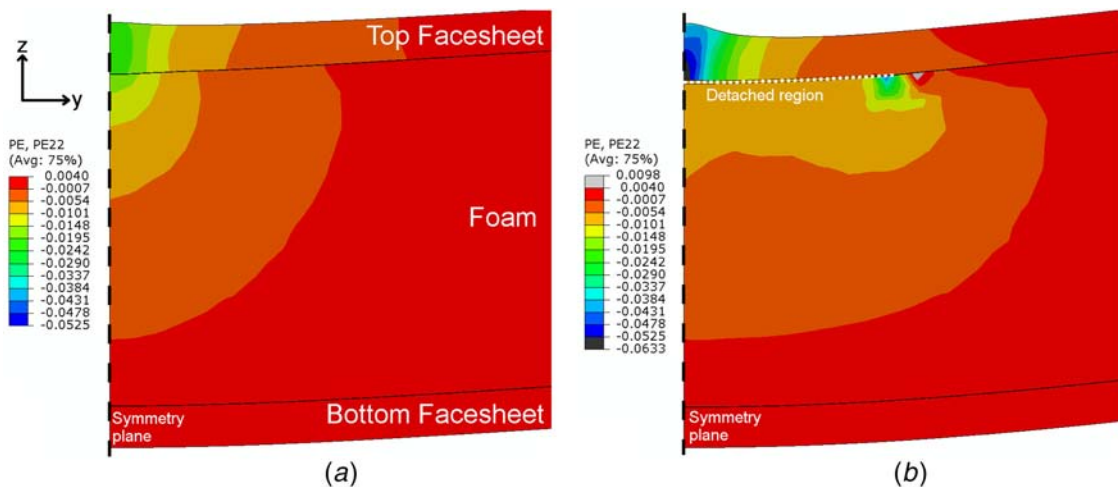

Fig. 17 Plastic strain distributions in the y-direction after a laser scan at a large spot size ($D = 12$ mm, $v = 10$ mm/s). In (a), the adhesion between the top facesheet and the foam core is intact, whereas in (b), the top facesheet is detached from the foam core over a half the spot size of $D = 12$ mm. Only half of the model is shown due to symmetry. The deformation was scaled by a factor of 10 for viewing clarity.

thickness of the sandwich panel and rendering it more resistant to bending deformation.

Overall, this study demonstrated that a large variety of metal foam sandwich panel types can be laser formed, provided that the bond between the facesheets and the foam core is sufficiently strong to withstand the high temperatures and stresses that develop during the process. The bending efficiency and limit depend on the interactions between the panel properties and process conditions. Using the understanding developed in this study, potential applications in industry can be further explored.

Acknowledgment

Nomenclature

e = emissivity
s = sandwich thickness
v = laser scan speed
w = specimen width
x = x-coordinate
y = y-coordinate
z = z-coordinate
A = absorption coefficient
D = laser beam diameter
F = yield surface parameter
G = interface conductance
H = hardening modulus
I = moment of area
P = laser power
R = radius of curvature
T = temperature
Y = yield strength
$\dot{Y}$ = rate of change of yield strength
h_σ = tangent modulus in uniaxial compression
h_p = tangent modulus in hydrostatic compression
s_i = thickness of layer i
t_n = normal traction
t_s = shear traction in first direction
t_t = shear traction in second direction
u_n = displacement in normal direction
u_s = displacement in first shear direction
u_t = displacement in second shear direction
y_i = y-displacement of layer i
z_i = z-displacement of layer i
E_0 = Young's Modulus of interface
E_i = Young's Modulus of layer i
G_0 = shear stiffness of interface
K_{nn} = stiffness in normal direction
K_{ss} = Stiffness in first shear direction
K_{tt} = Stiffness in second shear direction
M_i = bending moment at layer i
P_i = load at layer i
AE = area energy

α_i = thermal expansion coefficient of layer i
β = aspect ratio of the yield surface
ΔT = change in temperature
ε = strain
$\dot{\varepsilon}_{ij}^p$ = plastic strain rate
η = interface thickness
ρ = density
σ = stress
$\hat{\sigma}$ = equivalent stress
σ_e = Von Mises' Equivalent stress
σ_m = mean stress
τ = infinitesimal increment

References

[1] Ashby, M. F., Evans, A. G., Fleck, N. A., Gibson, L. J., Hutchinson, J. W., and Wadley, H. N. G., 2000, *Metal Foams: A Design Guide*, Butterworth-Heineman, Washington, DC.

[2] Banhart, J., and Seeliger, H. W., 2008, "Aluminium Foam Sandwich Panels: Manufacture, Metallurgy and Applications," Adv. Eng. Mater., **10**(9), p. 793.

[3] Banhart, J., and Seeliger, H. W., 2012, "Recent Trends in Aluminum Foam Sandwich Technology," Adv. Eng. Mater., **14**(12), pp. 1082–1087.

[4] Hebsur, M., Noebe, R., and Revilock, D., 2003, "Impact Resistance of Lightweight Hybrid Structures for Gas Turbine Engine Fan Containment Applications," J. Mater. Eng. Perform., **12**(4), pp. 470–479.

[5] Hanssen, A. G., Girard, Y., Olovsson, L., Berstad, T., and Langseth, M., 2006, "A Numerical Model for Bird Strike of Aluminium Foam-Based Sandwich Panels," Int. J. Impact Eng., **32**, pp. 1127–1144.

[6] Kennedy, A., 2012, *Powder Metallurgy, Porous Metals and Metal Foams Made from Powders*, InTech, Rijeka, Croatia, Chap. 2.

[7] D'Urso, G., and Maccarini, G., 2011, "The Formability of Aluminum Foam Sandwich Panels," Int. J. Mater. Form., **5**(3), pp. 243–257.

[8] Contorno, D., Filice, L., Fratini, L., and Micari, F., 2006, "Forming of Aluminum Foam Sandwich Panels: Numerical Simulations and Experimental Tests," J. Mater. Process. Technol., **177**(1–3), pp. 364–367.

[9] Mata, H., Santos, A., Parente, M., Valente, R., Fernandes, A., and Jorge, N., 2013, "Study on the Forming of Sandwich Shells With Closed-Cell Foam Cores," Int. J. Mater. Form., **7**(4), pp. 413–24.

[10] Bucher, T., Cardenas, S., Verma, R., Li, W., and Yao, Y. L., 2018, "Laser Forming of Sandwich Panels With Metal Foam Cores," ASME J. Manuf. Sci. Eng. **140**(11), p. 111015.

[11] Raj, S. V., Ghosn, L. J., Lerch, B. A., Hebsur, M., Cosgriff, L. M., and Fedor, J., 2007, "Mechanical Properties of 17-4PH Stainless Steel Foam Panels," Mater. Sci. Eng. A, **456**(1–2), pp. 305–316.

[12] Vollertsen, F., 1993, "The Mechanisms of Laser Forming," CIRP Ann., **42**(1), pp. 301–304.

[13] Abawi, A. T., 2004, "The Bending of Bonded Layers Due to Thermal Stress," Hughes Research Laboratories, Malibu, CA.

[14] Deshpande, V., and Fleck, N., 2000, "Isotropic Constitutive Models for Metallic Foams," J. Mech. Phys. Solids, **48**(6–7), pp. 1253–1283.

[15] Bucher, T., Young, A., Zhang, M., Chen, C. J., and Yao, Y. L., 2018, "Thermally Induced Mechanical Response of Metal Foam During Laser Forming," ASME J. Manuf. Sci. Eng., **140**(4), p. 041004.

[16] Bucher, T., Bolger, C., Zhang, M., Chen, C., and Yao, Y. L., 2016, "Effect of Geometrical Modeling on Prediction of Laser-Induced Heat Transfer in Metal Foam," ASME J. Manuf. Sci. Eng., **138**(12), p. 121008.

[17] Li, W., and Yao, Y. L., 2001, "Laser Forming With Constant Line Energy," Int. J. Adv. Manuf. Technol., **17**, pp. 196–203.

[18] Turon, A., Davila, C. G., Camanho, P. P., and Costa, J., 2007, "An Engineering Solution for Mesh Size Effects in the Simulation of Delamination Using Cohesive Zone Models," Eng. Fract. Mech., **74**(10), pp. 1665–1682.

[19] Spittel, T., Spittel, M., and Warlimont, H., 2011, *Non-ferrous Alloys – Light Metals Vol. VIII/2C2, AlSi8*, Springer, Berlin, Germany.

[20] Spittel, T., Spittel, M., and Warlimont, H., 2011, *Non-ferrous Alloys – Light Metals Vol. VIII/2C2, AlMg1*, Springer, Berlin, Germany.

[21] Spittel, T., Spittel, M., and Warlimont, H., 2011, *Non-ferrous Alloys – Light Metals Vol. VIII/2C2, Al 99.7*, Springer, Berlin, Germany.

[22] Yang, C. C., and Nakae, H., 2000, "Foaming Characteristics Control During Production of Aluminum Alloy Foam," J. Alloys Compd., **313**, pp. 188–191.

[23] Li, W., and Yao, Y. L., 2000, "Numerical and Experimental Study of Strain Rate Effects in Laser Forming," ASME J. Manuf. Sci. Eng., **122**(3), p. 445.

[24] Towns, J., Cockerill, T., Dahan, M., Foster, I., Gaither, K., Grimshaw, A., Hazlewood, V., Lathrop, S., Lifka, D., Peterson, G. D., Roskies, R., Scott, J. R., and Wilkins-Diehr, N., 2014, "XSEDE: Accelerating Scientific Discovery," Comput. Sci. Eng., **16**(5), pp. 62–74.